Available online at www.sciencedirect.com
ScienceDirect
Optics Communications 281 (2008) 2374–2379
OPTICS COMMUNICATIONS
www.elsevier.com/locate/optcom

Quarter-wavelength multilayer interference filter for terahertz waves

Withawat Withayachumnankul [a,b,*], Bernd M. Fischer [a], Derek Abbott [a]

[a] Centre for Biomedical Engineering and School of Electrical and Electronic Engineering, The University of Adelaide, Adelaide, SA 5005, Australia
[b] Department of Information Engineering, Faculty of Engineering, King Mongkut's Institute of Technology Ladkrabang, Bangkok 10520, Thailand

Received 26 October 2007; received in revised form 19 December 2007; accepted 20 December 2007

Abstract

This work presents a multilayer interference filter, suitable for operation with terahertz waves (T-rays). An analysis of the effect of the number of layers on the spectral response is given, with full measurement data including time-resolved signals, transmittances, and phase spectra. The silicon–air structure with a submillimeter thickness shows a stop-band between 0.2 and 0.5 THz, and the attenuation inside the stop-band increases in proportion to the number of layers in the structure. The measurement of the fabricated structure is in agreement with a characteristic matrix analysis.

PACS: 07.57.−c; 42.25.Hz; 42.79.Ci

Keywords: THz-TDS; T-rays; Terahertz; Interference filter; Characteristic matrix; Time-resolved signal

1. Introduction

Ultrafast broadband terahertz systems have opened up the previously inaccessible frequency range lying between millimetre waves and infrared [1]. Consequently, a range of T-ray components are required to manipulate the propagation of T-rays, inasmuch as optical components are required to control visible light, infrared, or ultraviolet. These components may comprise lenses, mirrors, parabolic mirrors, beam splitters, filters, polarisers, and so on. Most of the T-ray components directly adopt principles from optics. This is possible since the T-ray characteristics are quasi-optical [2].

One of the common wave-manipulating components is a filter. A number of T-ray filters have been realised to date, owing to the requirements of either conventional FTIR (Fourier transform infrared) spectroscopy [3] or astronomical observations [4]. These filters can be categorised into two major types, according to the applied optical power, as active or passive filters. An active T-ray filter offers more flexibility in frequency and/or energy tuning, but at the expense of complexity and cost. A passive filter, on the other hand, is less complicated, but also less flexible in terms of its function.

Several approaches to passive terahertz filters are available, for example, reststrahlen bands [5], particle scattering [6], photonic bandgap crystals [7,8], perforated metal sheets [9–13], and interference in a multilayer structure. A multilayer interference filter[1] is an attractive option because of its structural simplicity yet optical functionality. By using alternating thin films of T-ray transparent materials, with a proper index arrangement, full control over a particular frequency band is easily attainable. This work presents a

* Corresponding author. Address: Centre for Biomedical Engineering and School of Electrical and Electronic Engineering, The University of Adelaide, Adelaide, SA 5005, Australia. Tel.: +61 8 8303 6296.
E-mail address: withawat@eleceng.adelaide.edu.au (W. Withayachumnankul).

[1] For simplicity in the following context an interference filter refers to a multilayer interference filter and not other types of filters exploiting a similar interference mechanism. The same structure may be found in other optical functions, and/or called by different names such as multilayer periodic structure, dichroic filter, 1D photonic bandgap structure, 1D photonic crystal, Bragg mirror, dielectric mirror, etc.

0030-4018/$ - see front matter © 2008 Elsevier B.V. All rights reserved.
doi:10.1016/j.optcom.2007.12.094

study of the quarter-wavelength multilayer interference filter. The operating frequency range covers the frequency of most ultrafast T-ray systems, i.e. between 0.1 and 1.0 THz [14]. Importance is given to the operation in the transmission mode, and the effects of altering the number of filter layers on the transmittance profile. The study of these effects is possible as the submillimetre structure allows a rapid change of the layer arrangement. Characterisation of the fabricated filter by THz-TDS (terahertz time-domain spectroscopy) delivers a time-domain signal, rarely achievable by other spectroscopic modalities. This evolving time-domain signal reveals significant characteristics of the filter, in addition to the information obtainable from the transmittance profile.

This work is organised as follows: previous findings on T-ray multilayer interference structures are given in Section 2. Section 3 provides the principle of quarter-wavelength multilayer interference filter, including an analysis on a change in the response of the filter as a function of the number of structural layers. Design of a filter and experimental results are given in Section 4. The work ends with conclusion in Section 5.

2. Review of multilayer interference structures

For decades, FTIR spectroscopy has been widely employed in the study of materials in the frequency range around the mid-infrared [15]. Correspondingly, multilayer interference structures operative in this frequency range, made from a number of different materials and configurations, are widely available. Provided there is no absorption, the structure can be operated either as a filter or mirror dependent on the alignment, as the two functions are complementary. Some multilayer structures used as FTIR mirrors are, for example: zinc sulphide/polyethylene [16], silicon–air [17].

Similar multilayer structures are designed for T-rays, i.e. from 0.1 to 1.0 THz, and characterised by THz-TDS. A series of these designs are, for example: Styrolux™/PE and polyethylene/air [18], polypropylene/silicon [19], alumina/alumina-zirconia [20], polypropylene/polypropylene + TiO_2 [21]. These earlier studies focus on finding materials and fabrication techniques suitable for the operation of the multilayer structures in the T-ray frequency range. The fabricated structures are expected to be used as mirrors for short-range or indoor T-ray communication. Thus, particular interest is given to an economic material fabrication, which provides a structure with the highest reflectivity and broadest reflection band at any angle of incidence. Our work, on the other hand, studies the dependency of the structure's characteristics on the number of layers, when the structure is used as a filter in a transmission arrangement. A rapid change of the number of filter's layers is possible owing to the large scale and retrofittability design of the structure. An elegant equation is derived, showing a logarithmic relation between the number of layers and the attenuation within a stop-band. Furthermore, our work supplements full data of the filter's response in terms of time-domain signal and phase response. This serves to provide more insight into the operation of the filter, in addition to characterising the spectral transmittance.

3. Quarter-wavelength multilayer interference filters

A multilayer interference filter is composed of several dielectric layers with different indices of refraction. Cascading these layers to form a periodic structure appropriately, as shown in Fig. 1a, gives the transmittance profile in the stacking direction similar to that shown in Fig. 1b. As the name implies, it is the interference mechanism that controls shape and position of the pass-band and stop-band. Particularly, constructive interference is responsible for the pass-band, whereas destructive interference is responsible for the stop-band. To achieve any type of interference, at any desired frequency, the wave dispersion is the only parameter to be adjusted. This is made possible by means of proper material arrangement, given that each material is *non-dispersive*, i.e. has a constant index of refraction, in the frequencies of interest.

The following subsection briefly discusses the characteristic matrix method, which is required to analyse the response of a multilayer structure. Section 3.2 explains the required quarter-wavelength optical thickness condi-

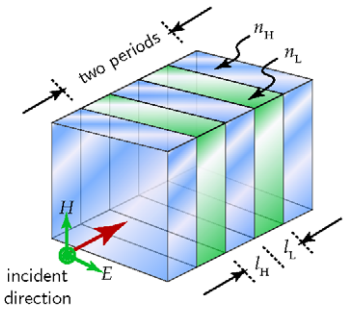

(a) periodic structure, 2.5 periods, $(HL)^2H$

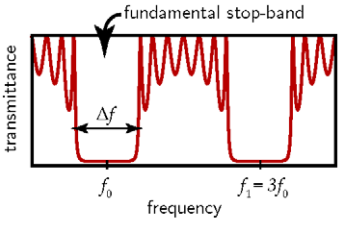

(b) corresponding transmittance

Fig. 1. Multilayer interference filter and its transmittance. (a) The structure comprises a number of dielectric periods. Each period is constructed from high- and low-indexed dielectric layers with the indices of refraction of n_H and n_L, and the thicknesses of l_H and l_L, respectively. The periodic structure usually starts and ends with a high-indexed material, and can be designated by $(HL)^aH$, where H and L symbolise high- and low-indexed materials, respectively, and a is the number of periods. (b) The transmittance of this periodic structure features spectrally distributed stop-bands. A fundamental stop-band has the central frequency of f_0 and the effective width of Δf.

tion. A mathematical relation, showing the effects of the number of periods in the structure on the filter response, is given in Section 3.3.

3.1. Characteristic matrix method

In order to analyse the response of the described periodic structure, the characteristic matrix method [22] is engaged. In brief, a characteristic matrix for high-indexed material, in the case that the wave propagation direction is parallel with the stacking direction, is given by

$$\mathbf{M}_H = \begin{bmatrix} \cos\left(\frac{\omega}{c} n_H l_H\right) & j\sin\left(\frac{\omega}{c} n_H l_H\right)/n_H \\ j n_H \sin\left(\frac{\omega}{c} n_H l_H\right) & \cos\left(\frac{\omega}{c} n_H l_H\right) \end{bmatrix}, \tag{1}$$

where n_H and l_H are the refractive index and the thickness attributed to a high-indexed material. Likewise, a matrix for the low-indexed material is

$$\mathbf{M}_L = \begin{bmatrix} \cos\left(\frac{\omega}{c} n_L l_L\right) & j\sin\left(\frac{\omega}{c} n_L l_L\right)/n_L \\ j n_L \sin\left(\frac{\omega}{c} n_L l_L\right) & \cos\left(\frac{\omega}{c} n_L l_L\right) \end{bmatrix}. \tag{2}$$

Here n_L and l_L are the refractive index and the thickness attributed to a low-indexed material. When slabs of these materials are layered using a periods, with the high-indexed material terminating both ends, the resulting characteristic matrix is simply obtainable via matrix multiplications in the proper order:

$$\mathbf{M}_{\text{total}} = \begin{bmatrix} m_{11} & m_{12} \\ m_{21} & m_{22} \end{bmatrix} = (\mathbf{M}_H \mathbf{M}_L)^a \mathbf{M}_H. \tag{3}$$

The transmission function of the structure in free space is calculated from the total characteristic matrix:

$$T(\omega) = \frac{2}{m_{11} + m_{12} + m_{21} + m_{22}}. \tag{4}$$

This transmission function, $T(\omega)$, is related to the transmittance, $\mathscr{T}(\omega)$, via $\mathscr{T}(\omega) = |T(\omega)|^2$.

3.2. Quarter-wavelength optical thickness

Essentially, due to the destructive interference from reflections, the transmittance of a dielectric slab with the refractive index n and thickness l is minimum at

$$f_N = (2N+1)\frac{c}{4nl}, \quad N = 0, 1, 2, \ldots. \tag{5}$$

This set of minima can be utilised for stop-bands of the filter. However, a single slab cannot cause a wide and deep enough stop-band. Thus, alternate cascading of a number of slabs made from two or more different materials, as illustrated in Fig. 1, is required. In order to enhance the stop-bands efficiently, the minima of those slabs must be at the same spectral position. This is made possible through an optical length equalisation:

$$n_H l_H = n_L l_L = \frac{c}{4f_0} = \frac{\lambda_0}{4}, \tag{6}$$

where again, the index of refraction and thickness of the high-indexed material are n_H and l_H, respectively, and those of the low-indexed material are n_L and l_L, respectively. From Eq. (6), the optical thickness, nl, of a material equals a quarter of the wavelength of the first minimum or the fundamental stop-band. Hence, this formulation leads to the term quarter-wavelength multilayer interference filter [22].

3.3. Effects of the number of periods on filter response

Each parameter of the structural design has effects on the filter spectral response in a unique way. The filter response, including the stop-band position, the width of the stop-band, and the attenuation inside a stop-band, are controlled via these parameters: the optical length of each layer, the step between high and low indices of refraction, and the number of periods. This section analyses the relation between the attenuation within a stop-band and the number of periods.

Consider the attenuation within a stop-band, in particular the attenuation at f_N, where $N = 0, 1, 2, \ldots$. Substituting the quarter-wavelength frequency, f_0, from Eq. (6) into Eqs. (1) and (2) yields, respectively:

$$\mathbf{M}_H = \begin{bmatrix} 0 & j/n_H \\ j n_H & 0 \end{bmatrix}, \quad \text{and} \quad \mathbf{M}_L = \begin{bmatrix} 0 & j/n_L \\ j n_L & 0 \end{bmatrix}. \tag{7}$$

The total matrix is therefore:

$$\mathbf{M}_{\text{total}} = (\mathbf{M}_H \mathbf{M}_L)^a \mathbf{M}_H = (-1)^a j \begin{bmatrix} 0 & n_L^a / n_H^{a+1} \\ n_H^{a+1} / n_L^a & 0 \end{bmatrix}, \tag{8}$$

where again, a is the number of periods in the filter. Following Eq. (4), the magnitude of the transmission function at f_0 is

$$|T(f_0)| = \frac{2}{n_L^a / n_H^{a+1} + n_H^{a+1} / n_L^a}. \tag{9}$$

In case that the difference between n_H and n_L is reasonably large, the above equation can be approximated to

$$|T(f_0)| \approx \frac{2}{n_H}\left(\frac{n_L}{n_H}\right)^a. \tag{10}$$

Taking a base-10 logarithm of the approximation results in

$$\log_{10}|T(f_0)| = a\log_{10}(n_L/n_H) - \log_{10}(n_H) + 0.3. \tag{11}$$

This relation is also applicable to the transmission at f_N, where $N = 1, 2, 3, \ldots$ and so on. It is obvious that the attenuation in the middle of a stop-band logarithmically depends on the number of periods, a. Also note that the attenuation at this frequency is independent of the physical thicknesses of the materials.

4. Experiment and result

4.1. Design of the silicon–air filters

Silicon and dry air are selected as materials for construction of the filter, owing to their low dispersion and absorp-

tion at T-ray frequencies. The first material, intrinsic high-resistivity float-zone (FZ) silicon, is known to have a negligible absorption and a constant refractive index of 3.418 at T-ray frequencies [23,24]. The second material, dry air, has a unity refractive index and nearly zero absorption for T-rays. Both silicon and air have no birefringence, and the optical properties of silicon in the T-ray regime are independent of the crystal orientation.

A batch of intrinsic FZ silicon wafers is supplied by Siltronix. Each wafer is polished on one side, has a resistivity of >1 kΩ, an orientation of ⟨1 1 1⟩, and a thickness of 50 ± 5 μm. Due to the Fabry–Pérot effect, or particularly the destructive interference, the transmission of a single wafer has a minimum at $f_0 = c/(4n_{si}l_{si}) = 0.439$ THz, given $n_{si} = 3.418$. This frequency is then set as the central frequency of the fundamental stop-band. The thickness of an air gap, $l_{air} = 170.9$ μm, is chosen to comply with the quarter-wavelength condition in Eq. (6). The width of a stop-band is estimated at 0.32 THz.

The material layers, comprising silicon wafers and air-rings, are fitted together by a HDPE (high-density polyethylene) frame, which exerts pressure on the structure via the elastic force of four identical springs. This spring-tight design helps reduce uneven forces at different surface positions and for different numbers of layers. Also it facilitates the replacement and retrofitting of material layers. The layout and design of the structure is given in Fig. 2.

4.2. Characteristics of the silicon–air filters

The THz-TDS system, used in characterisation of the filters, is a fibre-coupled T-ray Picometrix 2000, equipped with photoconductive antennas for T-ray generation and detection. The pumping laser is mode-locked Ti:Sa laser (MaiTai, Newport) with a central wavelength of 800 nm, a pulse duration of <80 fs, and a repetition rate of 80 MHz. The system produces T-ray pulses with a bandwidth from 0.1 to 1.0 THz and the maximum dynamic range of 25 dB. The T-ray beam passing through the filter is well collimated to avoid the difference in beam paths. The measurement for each filter is carried out nine times, and then the time-domain pulses are averaged. Also, the reference signal, measured with the same setting, is collected regularly to compensate amplitude drift effects within the system. For each recorded signal, the temporal window is 555.22 ps with a sampling interval of 33.9 fs. The Fourier transform of the pulse yields a spectral resolution of 1.8 GHz, and the reduction in system's bandwidth is not significant when the filter is in place.

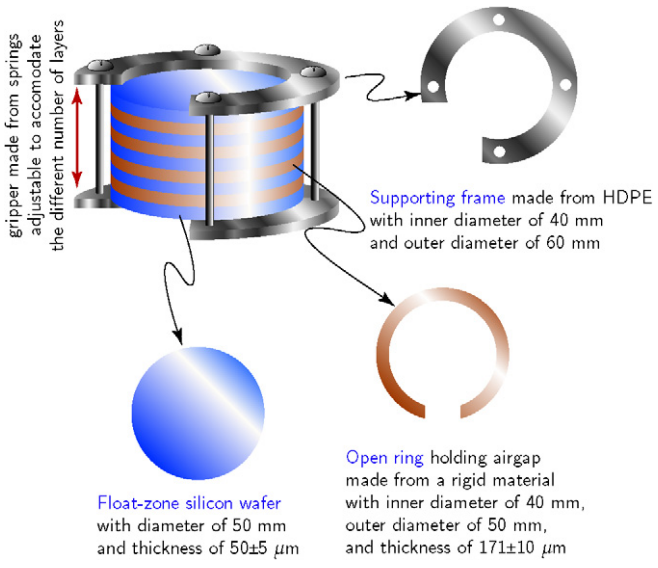

Fig. 2. Design of multilayer interference filter. The filter is composed of FZ silicon wafers alternating with air gaps, created by open rings. The materials are held together by a supporting frame made from high-density polyethylene (HDPE), and therefore the layers can be readily swapped in and out, or changed. The diameter of the structure is wide enough, so that the T-ray beam can pass through without edge diffraction.

Fig. 3 shows a set of pulses recorded from the silicon–air interference filters with various numbers of silicon–air periods. Determined from the first zero crossing point, each signal is delayed from its neighbour by 0.5 ps. The greater delays of the pulses are attributed to the increasing effective indices of refraction of the structures. The pulses for $(HL)^aH$ structures exhibit very little difference in the maximum amplitudes, which are approximately 40% of the reference amplitude. This is because the filters attenuate the amplitude at the specific frequency range while preserving the rest. However, the pulse shapes among the filters are largely distinctive. A possible likely cause is the spectral ripple in the pass-band, which is shown in the transmittance profiles (Fig. 4).

The transmittances in Fig. 4 are evaluated from the spectra of the reference, $E_{ref}(\omega)$, and of the filter, $E_{fil}(\omega)$, using $\mathcal{T}(\omega) = |E_{fil}(\omega)/E_{ref}(\omega)|^2$. From the figure, the first stop-band locates between 0.2 and 0.5 THz, the centre of which is at approximately 0.36 THz, and the FWHM is ≈0.3 THz. As the period of the filters increases, the attenuation in the middle of the stop-band increases logarithmically, roughly at an order of magnitude per period. This logarithmic relation confirms the theory in Eq. (11), and is plotted explicitly in Fig. 5. The filters have ripples in

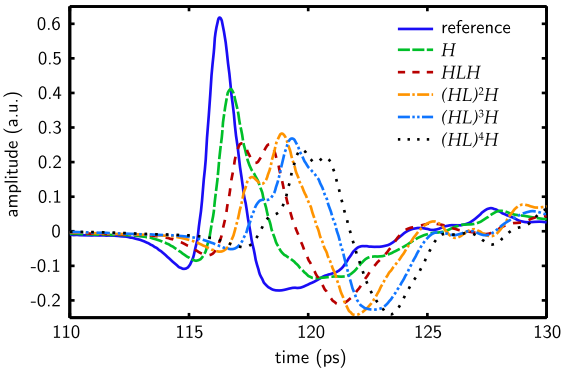

Fig. 3. T-ray signals transmitted through the interference filters. Only the signals inside the 20 ps window from the total recording duration of 555.22 ps are shown. The H measurement in fact represents the signal recorded from a single 50 μm silicon wafer. The pulses are delayed, attenuated, and reshaped by the filters.

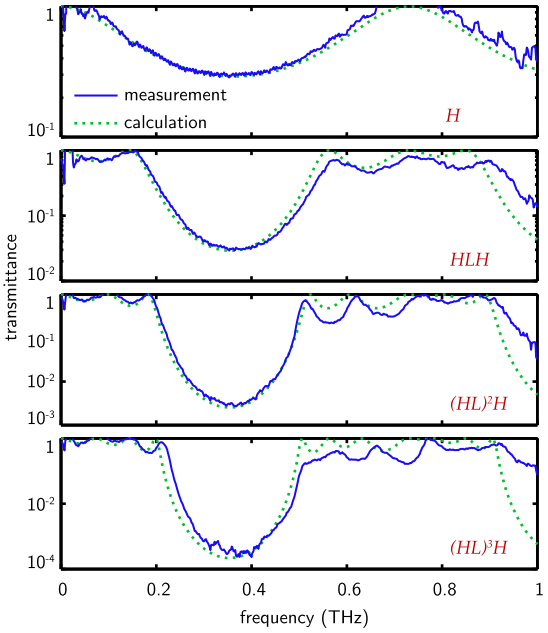

Fig. 4. Transmittance of the interference filters. For each filter, the first stop-band resides between 0.2 and 0.5 THz, centered at 0.36 THz. The successive stop-bands at higher frequencies are unresolvable due to the system bandwidth limit. The spectrum inside the stop-band of the $(HL)^3H$ filter is noisy, because the attenuation reaches the noise floor. The spectral transmittance for $(HL)^4H$ is not included, again due to the noise limit. The calculation is based on a characteristic matrix analysis. Notice the different ranges of the vertical scale.

the pass-band, i.e. between 0.0 and 0.2 THz, and between 0.5 and 0.9 THz, which are stronger following the number of periods. Due to the limited dynamic range of the system, it is not possible to render the second stop-band, which is beyond 0.9 THz.

The phase response is extracted using $\phi(\omega) = \angle E_{\text{fil}}(\omega) - \angle E_{\text{ref}}(\omega) - \omega L/c$. The $\omega L/c$ factor compensates the free space that occupies the structure's area with the thickness $L = a(l_H + l_L) + l_H$ in the reference measurement. The phase responses of the filters are shown in Fig. 6. It is clear that the phase is anomalous in the stop-band, in the 0.2–0.5 THz region.

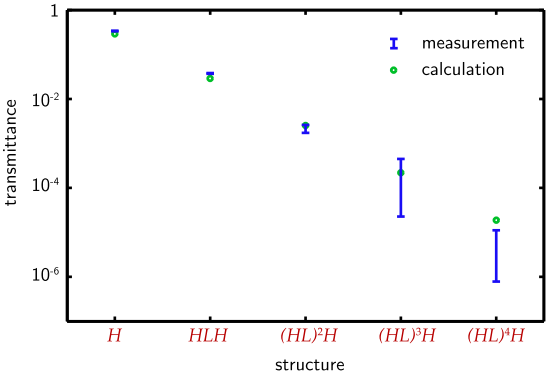

Fig. 5. Transmittance of the interference filters at 0.36 THz. The attenuation at the middle of the first stop-band increases logarithmically with the number of periods. The calculation is based on Eq. (11).

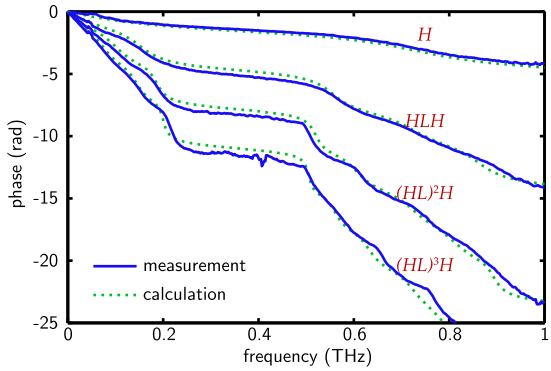

Fig. 6. Phase response of the interference filters. The phases are anomalous inside the stop-band, i.e. between 0.2 and 0.5 THz. The spectral phase of $(HL)^4H$ is not included here due to the limit of the system dynamic range. The calculation is based on a characteristic matrix analysis.

In spite of the appearance of the first stop-band, the central frequency of the stop-band deviates from the expectation at 0.439 THz. This is more likely due to uneven surfaces of the air gap rings, which result in thicker air layers. Hence, in the simulation, an adjustment to the material parameters is performed to compensate the structural thickness uncertainties. Through the fitting, using a characteristic matrix analysis [22], the thicknesses of the silicon wafers and air gaps are estimated at 60 μm and 220 μm, respectively, whereas their indices of refraction remain unchanged. The simulation results accompany the measured transmittances and phase responses in Figs. 4 and 6.

5. Conclusion and potential extensions

A set of the T-ray interference structures is designed to be operated as filter, in the transmission mode. Exploited in this work is a certain characteristic, namely the dependence of the stop-band attenuation on the number of filter layers. An explicit equation is derived, explaining the dependency in the logarithmic relation.

Realised according to the design, the filters are made from several ultrathin silicon wafers and air gaps, assembled in a novel retrofittable way. Characterised by transmission THz-TDS, the filters show an obvious stop-band spanning 0.2–0.5 THz with its central frequency at 0.36 THz. The transmittance in the stop-band decreases at approximately an order of magnitude per silicon–air period, as predicted by the theory. A characteristic matrix analysis shows an agreement between the model and the measurements at the estimated thicknesses of the silicon and air gap of 60 μm and 220 μm, respectively.

Acknowledgements

Thanks are due to Gretel Png, Brian Ng, and Samuel Mickan for useful discussion and to Ian Linke for his excellent technical assistance on the polyethylene frame.

References

[1] W. Withayachumnankul, G.M. Png, X.X. Yin, S. Atakaramians, I. Jones, H. Lin, B.S.Y. Ung, J. Balakrishnan, B.W.-H. Ng, B. Ferguson, S.P. Mickan, B.M. Fischer, D. Abbott, Proceedings of the IEEE 95 (8) (2007) 1528.

[2] P.F. Goldsmith, Proceedings of the IEEE 80 (11) (1992) 1729.

[3] P.R. Griffths, J. de Haseth, Fourier Transform Infrared Spectroscopy, Wiley, NY, 1986.

[4] J.S. Seeley, R. Hunneman, A. Whatley, Applied Optics 20 (1) (1981) 31.

[5] A.F. Turner, L. Chang, T.P. Martin, Applied Optics 4 (8) (1965) 927.

[6] K.R. Armstrong, F.J. Low, Applied Optics 13 (2) (1974) 425.

[7] E. Özbay, E. Michel, G. Tuttle, R. Biswas, K.M. Ho, J. Bostak, D.M. Bloom, Applied Physics Letters 65 (13) (1994) 1617.

[8] E. Özbay, E. Michel, G. Tuttle, R. Biswas, K.M. Ho, J. Bostak, D.M. Bloom, Optics Letters 19 (15) (1994) 1155.

[9] K.F. Renk, L. Genzel, Applied Optics 1 (5) (1962) 643.

[10] R. Ulrich, Applied Optics 7 (10) (1968) 1987.

[11] C. Winnewisser, F. Lewen, H. Helm, Applied Physics A: Materials Science and Processing 66 (6) (1998) 593.

[12] C. Winnewisser, F. Lewen, J. Weinzierl, H. Helm, Applied Optics 38 (18) (1999) 3961.

[13] C. Winnewisser, F.T. Lewen, M. Schall, M. Walther, H. Helm, IEEE Transactions on Microwave Theory and Techniques 48 (4) (2000) 744.

[14] D. Abbott, X.-C. Zhang, Proceedings of the IEEE: A Special Issue on T-Ray Imaging, Sensing and Retection 95 (8) (2007) 1509.

[15] P.R. Griffths, Science 222 (4621) (1983) 297.

[16] J. Shao, J.A. Dobrowolski, Applied Optics 32 (13) (1993) 2361.

[17] R. Schiwon, G. Schwaab, E. Bründermann, M. Havenith, Applied Physics Letters 83 (20) (2003) 4119.

[18] D. Turchinovich, A. Kammoun, P. Knobloch, T. Dobbertin, M. Koch, Applied Physics A: Materials Science & Processing 74 (2) (2002) 291.

[19] N. Krumbholz, K. Gerlach, F. Rutz, M. Koch, R. Piesiewicz, T. Kürner, D. Mittleman, Applied Physics Letters 88 (2006) 202905.

[20] F. Rutz, M. Koch, L. Micele, G. de Portu, Applied Optics 45 (31) (2006) 8070.

[21] C. Jansen, F. Neubauer, J. Helbig, D.M. Mittleman, M. Koch, Flexible Bragg reflectors for the terahertz regime composed of polymeric compounds, in: Conference Digest of the Joint 32th International Conference on Infrared and Millimeter Waves and 15th International Conference on Terahertz Electronics, Cardiff, UK, September, 2007, p. 984.

[22] E. Hecht, Optics, second ed., Addison-Wesley, 1987.

[23] D. Grischkowsky, S. Keiding, M. van Exter, C. Fattinger, Journal of the Optical Society of America B: Optical Physics 7 (10) (1990) 2006.

[24] J. Dai, J. Zhang, W. Zhang, D. Grischkowsky, Journal of the Optical Society of America B: Optical Physics 21 (7) (2004) 1379.